HHS Public Access

Author manuscript

Neuroimage. Author manuscript; available in PMC 2019 June 01.

Published in final edited form as:

Neuroimage. 2018 June ; 173: 3–12. doi:10.1016/j.neuroimage.2018.02.005.

Targeting Alpha-band Oscillations in a Cortical Model with Amplitude-Modulated High-Frequency Transcranial Electric Stimulation

Ehsan Negahbani[1], **Florian H Kasten**[6], **Christoph S Herrmann**[7,8], and **Flavio Frohlich**[1,2,3,4,5,6]

[1]Dept. of Psychiatry, Univ. of North Carolina, Chapel Hill, NC 27514-5307

[2]Dept. Cell Biology and Physiology, Univ. of North Carolina, Chapel Hill, NC 27514-5307

[3]Dept. of Biomedical Engineering, Univ. of North Carolina, Chapel Hill, NC 27514-5307

[4]Neuroscience Center, Univ. of North Carolina, Chapel Hill, NC 27514-5307

[5]Dept. of Neurology, Univ. of North Carolina, Chapel Hill, NC 27514-5307

[6]Carolina Center for Neurostimulation, Univ. of North Carolina, Chapel Hill, NC 27514-5307; Dept. of Psychology, Cluster for Excellence “Hearing for All”, European Medical School, Oldenburg, Germany

[7]Experimental Psychology Lab, Cluster for Excellence “Hearing for All”, European Medical School, Oldenburg, Germany

[8]Res. Ctr. Neurosensory Sci., Carl von Ossietzky Univ., Oldenburg, Germany

Abstract

Non-invasive brain stimulation to target specific network activity patterns, e.g. transcranial alternating current stimulation (tACS), has become an essential tool to understand the causal role of neuronal oscillations in cognition and behavior. However, conventional sinusoidal tACS limits the ability to record neuronal activity during stimulation and lacks spatial focality. One particularly promising new tACS stimulation paradigm uses amplitude-modulated (AM) high-frequency waveforms (AM-tACS) with a slow signal envelope that may overcome the limitations. Moreover. AM-tACS using high-frequency carrier signals is more tolerable than conventional tACS, e.g. in terms of skin irritation and occurrence of phosphenes, when applied at the same current intensities (e.g. 1-2 mA). Yet, the fundamental mechanism of neuronal target-engagement by AM-tACS waveforms has remained unknown. We used a computational model of cortex to investigate how AM-tACS modulates endogenous oscillations and compared the target engagement mechanism to

Corresponding author: Flavio Frohlich, flavio_frohlich@med.unc.edu.

Conflict of Interest

CSH has received honoraria as editor from Elsevier Publishers and filed a patent application for transcranial electric stimulation. FF is the founder, chief scientific officer, and majority owner of Pulvinar Neuro LLC.

the case of conventional (unmodulated) low-frequency tACS. Analysis of stimulation amplitude and strength indicated that cortical oscillations were phase-locked to the envelope of the AM stimulation signal, which thus exhibits the same target engagement mechanism as conventional (unmodulated) low frequency tACS. However, in the computational model substantially higher current intensities were needed for AM-tACS than for low-frequency (unmodulated) tACS waveforms to achieve pronounced phase synchronization. Our analysis of the carrier frequency suggests that there might be a trade-off between the use of high-frequency carriers and the stimulation amplitude required for successful entrainment. Together, our computational simulations support the use of slow-envelope high frequency carrier AM waveforms as a tool for noninvasive modulation of brain oscillations. More empirical data will be needed to identify the optimal stimulation parameters and to evaluate tolerability and safety of both, AM- and conventional tACS.

Keywords

Brain stimulation; computer simulation; target engagement; transcranial alternating current stimulation; tACS; amplitude modulation

1. Introduction

Transcranial alternating current stimulation (tACS) is a noninvasive brain stimulation method in which a weak sinusoidal current is applied through scalp electrodes. Today's mechanistic understanding of tACS is based on computational modeling and animal studies that suggest tACS modulates brain function by entraining the endogenous network oscillations (Deans, Powell et al. 2007, Radman, Su et al. 2007, Fröhlich and McCormick 2010, Ozen, Sirota et al. 2010, Reato, Rahman et al. 2010, Ali, Sellers et al. 2013, Herrmann, Rach et al. 2013, Reato, Rahman et al. 2013, Schmidt, Iyengar et al. 2014, Jackson, Rahman et al. 2016). Human studies using electroencephalography (EEG) have confirmed the modulation of cortical oscillation by tACS (Zaehle, Rach et al. 2010, Boyle and Frohlich 2013, Herrmann, Rach et al. 2013, Marshall and Binder 2013, Neuling, Rach et al. 2013, Helfrich, Schneider et al. 2014, Vossen, Gross et al. 2015, Herrmann, Strüber et al. 2016, Kasten, Dowsett et al. 2016, Kasten and Herrmann 2017). In addition, there is a growing literature on using tACS to understand the role of brain oscillations in behavior, cognition, and memory (Herrmann, Rach et al. 2013, Santarnecchi, Polizzotto et al. 2013, Fröhlich 2014, Lustenberger, Boyle et al. 2015, Chander, Witkowski et al. 2016, Fröhlich, Alagapan et al. 2016).

Novel transcranial electric stimulation paradigms, where a high-frequency waveform is amplitude modulated by a slow waveform, are emerging with the purpose of improving conventional tACS (Witkowski, Garcia-Cossio et al. 2016, Grossman, Bono et al. 2017). While the modulating frequencies are within the EEG frequency range in these novel methods, the high-frequency carrier signals have frequencies higher than the ones of the classical EEG frequency bands. Amplitude modulation (AM) stimulation was originally inspired by the envelope decoding properties of neurons in auditory, visual, and mechanosensory systems (Lundstrom and Fairhall 2006, Middleton, Longtin et al. 2006,

Longtin, Middleton et al. 2008, Mazzoni, Panzeri et al. 2008, Doelling, Arnal et al. 2014, Clarke, Longtin et al. 2015) due to nonlinear properties of the cell membrane (Goldman 1943). Several advantages of AM waveforms in comparison to conventional (unmodulated) low-frequency tACS have recently been proposed. AM-tACS was successfully utilized to separate the stimulation artifact and MEG signals (Witkowski, Garcia-Cossio et al. 2016) that would enable the design of feedback stimulation systems. Building on earlier work on interferential stimulation (Goats 1990, Fuentes, Armijo Olivo et al. 2016), AM stimulation waveforms produced by temporal interference of two high-frequency waveforms with slightly different frequencies has been proposed as a noninvasive deep brain stimulation method that does not affect the overlaying regions (Grossman, Bono et al. 2017). More recently, AM signals produced by temporal interference of two high-frequency waveforms with slightly different frequencies has been proposed as a noninvasive deep brain stimulation method that does not affect the overlaying regions (Grossman, Bono et al. 2017). This use of AM waveforms as a by-product of interferential stimulation goes back to earlier works by (Goats 1990, Fuentes, Armijo Olivo et al. 2016). Also, high-frequency transcranial waveforms might result in less skin sensation and phosphene perception in transcranial stimulation protocols (Turi, Ambrus et al. 2013, Chaieb, Antal et al. 2014). Motivated by these potentially fundamental advantages of AM-tACS waveforms, we used a computational model to elucidate the possible mechanisms underlying modulation of cortical oscillations by AM-tACS waveforms.

We evaluated the stimulus parameter landscape of AM-tACS and found that this stimulation interacted with neural population dynamics via entrainment, similar to the underlying mechanisms of unmodulated low-frequency tACS. We further identified that subthreshold intensities of AM-tACS were sufficient to cause moderate entrainment of cortical oscillations. However, substantially higher stimulation intensities were required compared to conventional (unmodulated) tACS to reach the same level of phase synchrony between the stimulation signal and ongoing oscillations.

2. Methods

2.1. Cortical model

The cortical model was composed of excitatory regular spiking pyramidal cells (PY) and fast spiking inhibitory interneurons (FS). We used the Izhikevich formalism for point neurons, which is an abstraction of the Hodgkin-Huxley model and a generalization of the quadratic integrate-and-fire neuron (Izhikevich 2007). The governing equations were

$$C\frac{dv}{dt} = k(v - v_r)(v - v_t) - u + I$$

$$\frac{du}{dt} = a\{b(v - v_r) - u\}$$

$$\text{if } v \geq v_{\text{peak}}, \quad \text{then } v \leftarrow c, \quad u \leftarrow u + d$$

where v was the membrane potential, u was the recovery variable, C was the membrane capacitance, v_r was the resting membrane potential, and v_t was the instantaneous threshold potential. The recovery rate constant was a. The spike cutoff value was v_{peak}, and the voltage reset value was c. Here the term I represented all currents entering the neuron including a direct current (dc) offset (I_{dc}), a noise term (I_{noise}), synaptic currents (I_{syn}), and a term that modelled the effect of stimulation on the membrane voltage (I_{stim}):

$$I = I_{\text{dc}} + I_{\text{syn}} + I_{\text{stim}} + I_{\text{noise}}$$

The Izhikevich model is capable of reproducing the spiking dynamics of most types of mammalian neurons (Izhikevich 2003), and was previously used in the context of transcranial brain stimulation (Reato, Rahman et al. 2010, Ali, Sellers et al. 2013). We modelled the PY as

$$100\frac{dv}{dt} = 0.7(v + 60)(v + 40) - u + I$$

$$\frac{du}{dt} = 0.03\{-2(v + 60) - u\}$$

$$\text{reset rule: if } v \geq +35, \quad \text{then } v \leftarrow -50, \quad u \leftarrow u + 100\,.$$

The FS were modeled as

$$20\frac{dv}{dt} = (v + 55)(v + 40) - u + I$$

$$\frac{du}{dt} = 0.2\{U(v) - u\}, \quad U(v) = \begin{cases} 0 & \text{when } v \leq v_b \\ 0.025(v + 55)^3 & \text{otherwise} \end{cases}$$

$$\text{reset rule: if } v \geq +25, \quad \text{then } v \leftarrow -45$$

characterizing non-pyramidal basket or chandelier inhibitory cells providing intra-laminar inhibition to PY (Izhikevich 2007). The PY fired tonic spikes with adapting frequency in response to injected dc pulses. The FS did not exhibit such spike frequency adaptation. The model of the PY was type I with a continuous current-frequency relationship. In contrast, the model of the FS was type II with discontinuous current-frequency relationship.

2.2. Model of stimulation

We used point neurons and modeled the effect of stimulation as a small current (I_{stim}) injected into PY (Fröhlich and McCormick 2010, Ali, Sellers et al. 2013). This approach captures the induced membrane polarization at the level of the soma due to external electric field application (Deans, Powell et al. 2007, Lafon, Rahman et al. 2016). PY were selected as the target of stimulation since their morphology makes them particularly responsive to applied electric fields (Lopez, Chan et al. 1991, Radman, Ramos et al. 2009). The amount of membrane polarization due to injected current is shown in Figure 1 A, indicating a ~6 mV depolarization prior to spike generation due to I_{inj}=34 pA. We studied the effect of applying a wide range of stimulation amplitudes in this paper, including but not limited to the subthreshold values that are used in transcranial electric stimulation protocols.

2.3. AM waveform

The waveform of AM-tACS was constructed by multiplying two sinusoidal waveforms according to

$$\mathrm{AM}_{\mathrm{stim}}(t) = a_{\mathrm{stim}}(\cos(2\pi f_m t) + 1)\sin(2\pi f_c t)$$

where a_{stim} was the stimulation intensity, f_m was the modulating frequency and f_c was the carrier frequency. Expanding the equation

$$\mathrm{AM}_{\mathrm{stim}}(t) = a_{\mathrm{stim}}\left[\frac{\sin(2\pi(f_c + f_m)t) + \sin(2\pi(f_c - f_m)t)}{2} + \sin(2\pi f_c t)\right]$$

denoted that AM-tACS was composed of three sinusoidal waves with frequencies at f_c and ($f_c \pm f_m$), see Figure 5 C (red traces) for time course and spectrum.

2.4. Synaptic connections

We used a computationally efficient, biophysical synaptic model. The synaptic current I_{syn} was

$$I_{\mathrm{syn}} = g(t)(V_{\mathrm{m}} - E_{\mathrm{rev}})$$

where $g(t)$ was the receptor conductance, was the postsynaptic membrane potential, and E_{rev} was the receptor-dependent reversal potential. Upon arrival of presynaptic action potential (AP) at the synaptic terminal, the conductance value was increased by g_{max}, then the conductance decayed exponentially as $g(t) = g_{t_{\mathrm{spike}}} \exp(-t/\tau)$ with τ as the corresponding time constant and $g_{t_{\mathrm{spike}}}$ as the synaptic conductance at the arrival time of presynaptic spike with g_{max} added. We assumed that the different synaptic currents entering a particular neuron sum linearly (Traub, Contreras et al. 2005). We considered only α-amino-3hydroxy-5-isoxazolepropionic acid (AMPA) and γ-aminobutyric acid type A

($GABA_A$) mediated synaptic current. The synaptic currents entering PY and FS were implemented as:

$$I_{\text{syn,PY}} = g_{\text{EE}}(t)(V_{\text{PY}} - E_{\text{AMPA}}) + g_{\text{IE}}(t)(V_{\text{PY}} - E_{\text{GABA}_A})$$

$$I_{\text{syn,FS}} = g_{\text{EI}}(t)(V_{\text{FS}} - E_{\text{AMPA}}) + g_{\text{II}}(t)(V_{\text{FS}} - E_{\text{GABA}_A})$$

where $E_{\text{AMPA}} = 0$ mV and $E_{\text{GABA}_A} = -70$ mV were the reversal potentials. Maximum conductances were $g_{\text{max,EE}} = 0.3$ nS, $g_{\text{max,EI}} = 0.4$ nS $g_{\text{max,IE}} = 0.3$ nS, $g_{\text{max,II}} = 0.03$ nS with corresponding time constants of $\tau_{\text{EE}} = \tau_{\text{EI}} = 2$ ms and $\tau_{\text{II}} = \tau_{\text{IE}} = 10$ ms.

2.5. Connectivity

The network was composed of 80 PY and 20 FS and both populations were spatially arranged on a line. The network had a connectivity pattern (Figure 1 B) inspired by the structure of neocortical neural circuits in Layer 5 (Markram, Toledo-Rodriguez et al. 2004, Harris and Shepherd 2015, Naka and Adesnik 2016). The coupling of PY exhibited an all-to-all structure with a connection probability of 50%. Each FS locally connected to 10 adjacent FS with a connection probability of 80%. Each FS was connected to 32 adjacent PY with a connection probability of 80%. We used a completely reciprocal local connection scheme for the PY-to-FS and FS-to PY connections (Yoshimura and Callaway 2005).

2.6. Local field potential model

We modelled the local field potential (LFP) signal by averaging the sum of the absolute values of AMPA and $GABA_A$ currents entering PY neurons

$$\text{LFP} = \sum_{i=1}^{N} \frac{\left|I_{\text{AMPA},i}\right| + \left|I_{\text{GABA}_A,i}\right|}{N}, \quad N: \text{number of PY neurons}$$

assuming that AMPA and $GABA_A$ currents both contribute in LFP signal with same sign (Mazzoni, Lindén et al. 2015). Based on the dendritic morphology, only the synaptic currents entering the excitatory neurons were considered to contribute to the generation of the LFP (Nunez and Srinivasan 2006, Mazzoni, Panzeri et al. 2008).

2.7. Modeling of cortical oscillations

To generate an endogenous, rhythmic activity pattern in the network, we adjusted the input currents to both the PY and FS. Specifically, we aimed to generate a cortical oscillation in the alpha frequency band (8-12 Hz) since these oscillations play a fundamental role in cognition (Klimesch 1999, Klimesch, Sauseng et al. 2007), and have been successfully targeted in a variety of tACS experiments in the past (Zaehle, Rach et al. 2010, Neuling, Rach et al. 2013, Vossen, Gross et al. 2015, Fröhlich 2016, Kasten, Dowsett et al. 2016, Kasten and Herrmann 2017). We note that our model simulates endogenous alpha-band

activity in a local cortical circuit. The model does not capture the circuit dynamics and structural and functional connectivity of the thalamo-cortical system that generates alpha rhythms (Da Silva, Van Lierop et al. 1973, Hughes and Crunelli 2005, Saalmann, Pinsk et al. 2012, Hawkins 2016). Rather, we aimed to only match the frequency of the model to alpha-band oscillations and focus on the mechanism of interaction between an endogenous neural rhythm and an external stimulation. Our results need to be tested in a comprehensive model of thalamocortical alpha oscillations and experimental setups. To generate the endogenous oscillations, we first determined the depolarizing current needed to cause 10 Hz firing in an isolated PY ($I_{dc,PY}$ = 79 pA). Then, we adjusted the current injected into FS to a value that brought isolated FS close to the threshold for action potential generation ($I_{dc,FS}$ = 60 pA). Once connected to form a network, spontaneous oscillatory activity emerged with frequency of 10 Hz in the simulated LFP.

Gaussian noise with zero mean and standard deviation of σ = 0.1 pA (I_{noise}) was added to the dc input of all neurons to model the subthreshold afferent inputs. Heterogeneity was added to individual neurons by adding a 1% jitter drawn from a normal distribution to the model parameter values. The network was implemented using the Brian package in Python (Goodman and Brette 2009), using the fixed-step Euler method with a time step of dt = 0.5 ms.

2.8. Data analysis

We used the Chronux toolbox (Mitra and Bokil 2008) to analyze the LFP signal in the frequency domain using the multi-taper method (Percival and Walden 1993). For the multi-taper analysis, the time-bandwidth product and the number of tapers were selected as 3 and 5 respectively (findings were robust to changes in these parameters). We used the phase-locking value (PLV) to quantize the entrainment of the LFP and individual neurons by the stimulation signal (Lachaux, Rodriguez et al. 1999). PLV analysis does not rely on stationarity of signals and PLV provides a more accurate estimation of synchrony when compared with spectral coherence (Lowet, Roberts et al. 2016). To compute PLV, we extracted the instantaneous phases of LFP and stimulation signals using the Hilbert-Transform (HT) which converts a real-valued signal to a complex signal from which the phase can be computed (Gabor 1946). We noticed that the simulated LFP was lacking the characteristic $1/f$ structure and always had a narrow-band structure centered on the endogenous frequency (Figure 2E) or two narrow bands on the endogenous and the stimulation frequencies when the network was stimulated (Figure 3A, B, C, spectrograms). Given the limitations of reliable bandpass filtering of low frequency signals, we used empirical mode decomposition (EMD) instead of Fourier-based band-pass filtering (Huang 2014). Using an iterative method, the EMD decomposes a signal to its intrinsic mode functions. Each intrinsic mode is shown to be a mono-frequency signal (Huang, Shen et al. 1998) for which the Hilbert transform can be applied to extract the corresponding instantaneous phase and frequency (Boashash 1992). We first applied the HT to each intrinsic mode, and extracted the corresponding instantaneous phases. The instantaneous frequency of each mode then computed as the scaled (divided by the sampling frequency) derivative of instantaneous phase. We finally assigned a mean frequency for each intrinsic mode using the mean value of corresponding instantaneous frequencies. The intrinsic mode

with closest frequency to stimulation frequency was selected for PLV analysis. Next step was to extract the phase of stimulation waveform. For conventional tACS, the HT was applied directly to the sinusoidal signal, and for AM-tACS the HT was applied to the envelope of the stimulation signal for phase extraction. The PLV value was calculated as

$$\mathrm{PLV} = \frac{1}{N}\left|\sum_{n=1}^{N} e^{j(\varphi_A(n) - \varphi_B(n))}\right|$$

where $\varphi_A(n) - \varphi_B(n)$ is the instantaneous phase difference between the LFP and stimulation signals at instance n, and N represents the total number of samples. Due to band-limited nature of simulated LFP signal, the resulting PLVs are much closer to 1 (indicative of complete phase locking) when compared to PLV of their realistic counterparts in EEG or LFP studies.

3. Results

3.1. Endogenous network activity and phase locking to conventional tACS

We first examined the network activity in the absence of any external stimulation. The sustained rhythmic activity in both individual neurons and at the population level resulted in an LFP signal with a dominant spectral peak at f_{end} = 10 Hz (Figure 2).

We next simulated the network for 40 seconds while applying conventional tACS with three different frequencies (less than, equal and more than the endogenous frequency; 10 Hz ± 3.5 Hz) for 20 seconds (starting at t = 10 s). The tACS amplitude was set to a subthreshold value (25 pA) that depolarizes individual neurons without driving action potentials (Figure 3 left column). The LFP spectrogram showed ongoing oscillations at 10 Hz before and after the application of stimulation (Figure 3, right column, arrows). Individual neurons aligned their spiking activity in response to stimulation (blue dots in Figure 3, raster plots). The modulation of ongoing activity was evident upon application of conventional tACS. The 6.5 Hz and 13.5 Hz stimuli shifted the frequency of the ongoing oscillations (Figure 3A, C). The 10 Hz stimulation amplified the ongoing oscillations without a frequency shift (Figure 3B). Of note, the spectral power during stimulation was the highest for the 10 Hz stimulation that matched the endogenous frequency of the network.

Given that the response magnitude depended on the stimulation frequency, we performed further comprehensive analysis by stimulating the cortical model with a full set of not only stimulation frequencies and but also intensities. We inspected the resulting interactions that revealed the phase locking of cortical oscillations to conventional tACS. For each trial, we simulated the network for 8 seconds, extracted the LFP signal, computed the PLV between stimulation and LFP and demonstrated the color-coded PLV value on the frequency-intensity plot (Figure 4 A, B). Triangular high-PLV zones emerged indicative of the synchronization regions known as Arnold tongues for a system of a coupled oscillator and an external force (Jensen, Bak et al. 1983, Pikovsky, Rosenblum et al. 2003). The existence of triangular synchronization regions has been previously shown for an external stimulation and a network of model neurons (Reato, Rahman et al. 2010, Ali, Sellers et al. 2013, Herrmann,

Murray et al. 2016). The high-PLV regions were aligned to 10 Hz (endogenous frequency) and its harmonics. The dashed line at $I = 34$ pA divides the map to subthreshold and superthreshold regions. This line represents the threshold value for the constant current stimulation intensity to elicit action potentials in synaptically-isolated PYs. While we explored both regimes, subthreshold stimulation models the weak input provided by conventional tACS. The triangular region at the first harmonic had a breakage around 20 Hz characterized by lower PLV than the neighboring regions (Figure 4 A). We performed further analysis of the network dynamics within and just outside of this breakage zone by looking at the spiking activity and their phase locking to stimulation. At the breakage the stimulation at [21 Hz, 44.1 pA] induced synchronous 10 Hz firing across individual PY and FS and the resultant LFP (Figure 4 A, open white circle (C), and Figure 4 C). The individual PY and FS fired in synchrony at 10 Hz resulting in a 10 Hz population oscillations and a dominant 10-Hz oscillation in resultant LFP. In contrast, the 10 Hz oscillation was not evident for an adjacent point outside of the breakage such as [23 Hz, 44.1 pA] (Figure 4 A, open white circle (D), and Figure 4 D). While the individual neurons were still firing around 10 Hz, the population activity and the resulting LFP was at ~23 Hz, the frequency of stimulation. The peak-frequency heat map of the LFP signal also confirmed the 10-Hz LFP oscillations for tACS frequencies close to 21 Hz (Figure 4 E, white arrow). Together, these results show a dissociation of network and single-cell oscillation frequency for stimulation that is not exactly tuned to the harmonic of the endogenous frequency. Next, we analyzed the synchronization in single-neuron level by computing the phase locking between individual neurons and conventional tACS. The analysis revealed the existence of triangular regions in the stimulation parameter space. These entrainment maps are shown for two randomly selected pyramidal neurons in Figure 4 F, G. In addition to triangular high-PLV regions around the endogenous frequency of individual neurons (~ 10 Hz), clear sub-harmonics and higher harmonics of the main Arnold tongue were also evident. Taken all together these results are indicative of ongoing interaction between cortical dynamics and unmodulated low-frequency tACS via phase locking mechanism at both the individual and the population level.

3.2. Entrainment of ongoing activity by the envelope of high frequency stimulation

We tested if comparable phase locking between the stimulation and network dynamics was achievable for conventional tACS and AM-tACS. In a series of three experiments, we simulated the network without stimulation, with conventional tACS and with AM-tACS. The network showed ongoing alpha band oscillations in the absence of stimulation (Figure 5 A). The application of unmodulated low-frequency tACS (10 Hz, 1.25 pA) amplified the power of endogenous oscillations and resulted in PLV=0.81 (Figure 5 B). We next applied AM-tACS with modulating and carrier frequencies of (f_m, f_c) = (10, 70) Hz respectively and adjusted the stimulation intensity to reach comparable entrainment as obtained via conventional tACS (Figure 5 C). We computed the phase locking of network oscillations relative to the phase of the modulating frequency and found that the stimulation intensity of $a_{\text{stim}} = 118.5$ pA was required to achieve PLV = 0.81. These results indicated that like conventional tACS, AM-tACS was also capable of entraining the network but a much larger super-threshold stimulation amplitude was required to induce the same level of entrainment. We further compared 10 Hz unmodulated tACS and 10 Hz AM-tACS ($f_c = 70$ Hz), and

extracted the PLV versus stimulation intensity traces for these two stimulation types (Figure 5D). Unlike the conventional tACS, the entrainment by AM-tACS was limited to phase locking values of PLV<0.2 in the subthreshold stimulation intensities as indicated by dashed line at I_{stim} = 34 pA.

To identify a complete entrainment map, we stimulated the model with AM-tACS (covering a wide range of modulating frequencies and stimulation intensities) and measured resultant PLV between the modulating frequency of stimulation and the LFP signal. The maps were extracted for carrier frequencies of f_c = 70 Hz and f_c = 200Hz (Figure 6 A, B respectively). For f_c = 70 Hz, high-PLV regions emerged and centered at f_{end} = 10 Hz, in the proximity of the subharmonic (~2.5 Hz and 5 Hz), and the harmonics (20 Hz and 30 Hz) indicating the existence of synchronization between AM-tACS and neural population. The circular histogram of phase differences between stimulation and LFP was also plotted at selected, qualitatively different points of the parameter space. While the high-PLV region appeared as a triangular shape around the endogenous frequency, the shape was relatively irregular around subharmonic and harmonics. Comparing with the corresponding entrainment map for conventional tACS (Figure 4), the regions with high PLV were shifted upward and required stimulation amplitudes above spiking threshold (Figure 6A, dashed line) and covered smaller areas on the map.

The second entrainment map was extracted for a higher carrier frequency at f_c = 200 Hz (Figure 6B) to study the effect of the carrier frequency. We did not find triangular shaped high PLV regions even for stimulation intensities beyond the spiking threshold of individual neurons. Rather, the triangular high-synchrony areas were replaced with narrow bands centered along f_{end} = 10 Hz and its harmonics with low phase locking values (PLV < 0.45).

3.3. Effect of high frequency carrier wave

We further stimulated the cortical model with fixed modulating frequency at f_m = 10 Hz but different stimulation amplitudes and carrier frequencies to clarify the effect of the carrier frequency. Higher carrier frequencies required higher intensities to entrain the network with high phase locking values (shades of orange and red (Figure 7 A).

To further evaluate the effect of carrier frequency, we extracted the spectral energy of the LFP signal under AM-tACS. The modulating frequency was again set to f_m = 10 Hz and different carrier frequencies and intensities were applied. The spectral energy around endogenous alpha-band oscillations was calculated as the area under the LFP spectrum within a 10 ± 2 Hz frequency band. We found that the higher carrier frequencies resulted in less spectral energies of LFP signal around the stimulation frequency (Figure 7 B).

4. Discussion

The underlying mechanisms by which AM-tACS modulates ongoing brain oscillations are widely unknown. Using a cortical model, here we demonstrate for the first time how the amplitude, and the modulation and carrier frequencies of an AM waveform influence its interaction with simulated ongoing cortical oscillations. This novel waveform has recently been proposed to address basic limitations of today's transcranial electrical stimulation

methods such as the elimination of the stimulation artifact and the localized targeting of deep brain regions (Witkowski, Garcia-Cossio et al. 2016, Grossman, Bono et al. 2017). Using a computational model of cortical network, we explored the parameter space of AM-tACS and compared the subsequent synchronization map with those of conventional tACS. We found that like conventional (unmodulate) low-frequency tACS, AM-tACS interacted with ongoing cortical oscillations via phase-locking mechanisms, demonstrated by high-synchrony regions in the stimulation parameter space. Our modeling study also revealed some limitations of AM-tACS, when compared to unmodulated low-frequency tACS. The former required higher stimulation intensities to reach PLVs comparable to the ones of conventional tACS. In addition to the modulating frequency and the intensity of the stimulation, we also found that the carrier frequency of AM-tACS played a major role in shaping the resultant phase-locking: increasing f_c demanded larger stimulation amplitudes to reach strong synchrony between stimulation and cortical oscillations. Our spectral analysis of the simulated cortical signal revealed attenuated transferred energy around envelope frequency for higher carrier frequencies. Taken together, although higher f_c values are preferred to maximize the spectral separation between stimulation and EEG for artefact removal and less peripheral sensations, our modeling results predict practical limitations of using higher frequencies and empirical data are required to test these predictions in real-world considerations. We did not repeat the simulations for different endogenous frequencies. Assuming the identical underlying mechanism for generation of local cortical circuit's endogenous rhythms (simulated by the Izhikevich formalism in our model), the reported findings should exhibit the same qualitative validity for different endogenous frequencies. However, our model does not include cortico-subcortical circuit dynamics that were shown to differ across different frequency bands.

Our modeling results are in agreement with previous slice electrophysiology work that showed a reduced response to sine wave electric fields with higher frequencies caused by low-pass filtering by the cell membrane capacitance (Deans, Powell et al. 2007). A recent in vivo study has reported the successful entrainment of ongoing oscillations using a small intensity interferential stimulation (Grossman, Bono et al. 2017). Direct translation of our results to those of Grossman et al. is not trivial. Part of their findings showing inefficacy of a single 2kHz stimulation source in entraining brain oscillations is in agreement with our predictions. However, our results do not explain how an AM-tACS waveform produced by the interference of two weak high-frequency waves can entrain neural oscillations. The lack of proposed AM-encoding circuitry of sensory cortex in our theoretical model may describe the discrepancy in our theoretical predictions and the entrainment reported in (Grossman, Bono et al. 2017). A recent study shows that a weak conventional tACS (0.05 mA) can result in comparable effects as standard intensities of conventional tACS (Ruhnau, Neuling et al. 2016). This further indicates that there are other unknown factors that are not included in our model and are responsive to high-frequency weak transcranial stimulation. In humans, application of unmodulated tACS with frequencies higher than the EEG frequency range increased the motor cortex excitability (Chaieb, Antal et al. 2011) while being safe to apply albeit at low amplitudes (Chaieb, Antal et al. 2014). The peripheral sensations were also reduced with increased stimulation frequency (Turi, Ambrus et al. 2013). Indeed, none of these human studies has reported entrainment of ongoing brain oscillations using those high-

frequency sinusoidal stimuli. Our entrainment map for conventional tACS predicts that while high-frequency unmodulated tACS centered at higher order harmonics of ongoing brain oscillations might entrain it, again significantly higher intensities are required for comparable PLVs with unmodulated tACS within EEG frequency range. This requirement also proposes practical limitation for using high-frequency unmodulated tACS to efficiently entrain endogenous brain oscillations. Our theoretical predictions should be tested and validated by empirical data before being translated to real-world considerations.

As any scientific study, our work has several limitations. First we acknowledge that our model does not include a thalamo-cortical loop that is proposed to be the basis for alpha activity (Da Silva, Van Lierop et al. 1973, Hughes and Crunelli 2005, Saalmann, Pinsk et al. 2012). The results we presented are based on the simulated endogenous alpha-band activity of a local cortical area, and translation of the results to alpha oscillations remains to be examined in comprehensive thalamocortical models and future in vivo or human studies. Second, we note that our frequency map had slightly different properties from that of a simple periodically-forced oscillator. A forced oscillator is known to oscillate at the stimulation frequency within a triangular region of the stimulation parameter space centered on the endogenous frequency. At the harmonics of the endogenous frequency, such an oscillator entrains to frequencies centered on the endogenous frequency, a phenomenon referred to as 1:2 entrainment for the first harmonic. In other words, if the oscillator has an endogenous frequency of 10 Hz, stimulation at 20 Hz and frequencies around it entrains the oscillator at frequencies around 10 Hz (Pikovsky, Rosenblum et al. 2003). Our results were in agreement with these theoretical predictions as displayed in f_{peak} map of LFP signal for the narrowband breakage at the harmonic of endogenous frequency (Fig. 4 E, white arrow). However, the broader triangular region centered on the first harmonic of the endogenous frequency correspond to entrainment at the stimulation frequency and thus twice the frequency of what the model of the forced oscillation would predict. Interestingly, however, individual neurons are more closely in agreement with the behavior of forced oscillators (Figure 4 C, D, F, and G). This suggests that the network interactions cause emergent synchronization at fast frequencies that allows the network to follow fast input in the form of stimulation or other afferent drive. Third, we did not study the possibility of stimulation-related aftereffects that might be explained by stimulation-induced modulation in neural plasticity mechanisms (Tergau and Paulus 2008, Zaehle, Rach et al. 2010, Reato, Bikson et al. 2015, Vossen, Gross et al. 2015).

5. Conclusions

In summary, we demonstrated how stimulation parameters of AM-tACS affects entrainment of alpha-band oscillations in a computational model of cortex. Despite the overall similarity of the target engagement mechanisms by unmodulated low-frequency tACS and AM-tACS, we found differences in their entrainment efficiency. While moderate intensities of conventional tACS resulted in strong phase-locking, similar intensities of AM-tACS only resulted in weak entrainment. For both types of paradigms, we showed how higher frequencies demanded higher intensities to result in strong phase synchronization. We also found that altering the endogenous network frequency using AM-tACS was limited to a narrower frequency band centered on the endogenous frequency when compared to

conventional tACS. In conclusion, our simulation suggests that AM-tACS is effective to target corticaloscillations in the human brain, but may require higher stimulation intensities for achieving the same level of phase synchrony between the stimulation signal and ongoing oscillations as compared to conventional unmodulated tACS. Further empirical data is required to test and validate our findings.

Acknowledgments

CSH was supported by the German Research Foundation (DFG, grant HE3353/8-2). Research reported in this publication was supported in part by the National Institute of Mental Health of the National Institutes of Health under award numbers R01MH111889 and R01MH101547. The content is solely the responsibility of the authors and does not necessarily represent the official views of the National Institutes of Health. The authors thank Dr. Craig Henriquez for assistance with the modeling code.

Abbreviations

tACS	transcranial alternating current stimulation
AM	amplitude modulation
AM-tACS	amplitude modulated transcranial current stimulation
EEG	electroencephalography
PY	pyramidal cells
FS	fast spiking cells
AMPA	α-amino-3hydroxy-5-isoxazolepropionic acid
$GABA_A$	γ-aminobutyric acid type A
LFP	local field potential
PLV	phase locking value
HT	Hilbert transform

References

Ali MM, Sellers KK, Frohlich F. Transcranial alternating current stimulation modulates large-scale cortical network activity by network resonance. The Journal of neuroscience : the official journal of the Society for Neuroscience. 2013; 33(27):11262–11275. [PubMed: 23825429]

Ali MM, Sellers KK, Fröhlich F. Transcranial alternating current stimulation modulates large-scale cortical network activity by network resonance. The Journal of Neuroscience. 2013; 33(27):11262–11275. [PubMed: 23825429]

Boashash B. Estimating and interpreting the instantaneous frequency of a signal. II. Algorithms and applications. Proceedings of the IEEE. 1992; 80(4):540–568.

Boyle MR, Frohlich F. EEG feedback-controlled transcranial alternating current stimulation. Neural Engineering NER, 2013 6th International IEEE/EMBS Conference on, IEEE. 2013

Chaieb L, Antal A, Paulus W. Transcranial alternating current stimulation in the low kHz range increases motor cortex excitability. Restorative neurology and neuroscience. 2011; 29(3):167–175. [PubMed: 21586823]

Chaieb L, Antal A, Pisoni A, Saiote C, Opitz A, Ambrus GG, Focke N, Paulus W. Safety of 5 kHz tACS. Brain stimulation. 2014; 7(1):92–96. [PubMed: 24064065]

Chander BS, Witkowski M, Braun C, Robinson SE, Born J, Cohen LG, Birbaumer N, Soekadar SR. tACS Phase Locking of Frontal Midline Theta Oscillations Disrupts Working Memory Performance. Frontiers in cellular neuroscience. 2016; 10

Clarke SE, Longtin A, Maler L. Contrast coding in the electrosensory system: parallels with visual computation. Nature Reviews Neuroscience. 2015

Da Silva FL, Van Lierop T, Schrijer C, Van Leeuwen WS. Organization of thalamic and cortical alpha rhythms: spectra and coherences. Electroencephalography and clinical neurophysiology. 1973; 35(6):627–639. [PubMed: 4128158]

Deans JK, Powell AD, Jefferys JGR. Sensitivity of coherent oscillations in rat hippocampus to AC electric fields. The Journal of Physiology. 2007; 583(Pt 2):555–565. [PubMed: 17599962]

Doelling KB, Arnal LH, Ghitza O, Poeppel D. Acoustic landmarks drive delta–theta oscillations to enable speech comprehension by facilitating perceptual parsing. Neuroimage. 2014; 85:761–768. [PubMed: 23791839]

Fröhlich F. Endogenous and exogenous electric fields as modifiers of brain activity: rational design of noninvasive brain stimulation with transcranial alternating current stimulation. Dialogues Clin Neurosci. 2014; 16(1):93–102. [PubMed: 24733974]

Fröhlich, F. Network Neuroscience. Elsevier; 2016.

Fröhlich, F., Alagapan, S., Boyle, MR., Hamilton, F., Li, G., Lustenberger, C., Schmidt, SL. Transcranial Direct Current Stimulation in Neuropsychiatric Disorders. Springer; 2016. Target Engagement with Transcranial Current Stimulation; p. 197-222.

Fröhlich F, McCormick DA. Endogenous electric fields may guide neocortical network activity. Neuron. 2010; 67(1):129–143. [PubMed: 20624597]

Fuentes JP, Armijo Olivo S, Magee DJ, Gross DP. Effectiveness of interferential current therapy in the management of musculoskeletal pain: a systematic review and meta-analysis. Physical therapy. 2016; 90(9):1219–1238.

Gabor D. Theory of communication. Part 1: The analysis of information. Journal of the Institution of Electrical Engineers-Part III: Radio and Communication Engineering. 1946; 93(26):429–441.

Goats G. Interferential current therapy. British journal of sports medicine. 1990; 24(2):87. [PubMed: 1702337]

Goldman DE. Potential, impedance, and rectification in membranes. The Journal of General Physiology. 1943; 27(1):37–60. [PubMed: 19873371]

Goodman DF, Brette R. The brian simulator. Frontiers in neuroscience. 2009; 3:26.

Grossman N, Bono D, Dedic N, Kodandaramaiah SB, Rudenko A, Suk HJ, Cassara AM, Neufeld E, Kuster N, Tsai LH. Noninvasive Deep Brain Stimulation via Temporally Interfering Electric Fields. Cell. 2017; 169(6):1029–1041.e1016. [PubMed: 28575667]

Harris KD, Shepherd GM. The neocortical circuit: themes and variations. Nature neuroscience. 2015; 18(2):170–181. [PubMed: 25622573]

Hawkins, K. Visual cortical alpha rhythms: function and relation to other dynamic signatures in local networks. University of Hull and the University of York; 2016.

Helfrich RF, Schneider TR, Rach S, Trautmann-Lengsfeld SA, Engel AK, Herrmann CS. Entrainment of brain oscillations by transcranial alternating current stimulation. Current Biology. 2014; 24(3): 333–339. [PubMed: 24461998]

Herrmann CS, Murray MM, Ionta S, Hutt A, Lefebvre J. Shaping intrinsic neural oscillations with periodic stimulation. The Journal of Neuroscience. 2016; 36(19):5328–5337. [PubMed: 27170129]

Herrmann CS, Rach S, Neuling T, Strüber D. Transcranial alternating current stimulation: a review of the underlying mechanisms and modulation of cognitive processes. Frontiers in human neuroscience. 2013; 7

Herrmann CS, Strüber D, Helfrich RF, Engel AK. EEG oscillations: from correlation to causality. International Journal of Psychophysiology. 2016; 103:12–21. [PubMed: 25659527]

Huang, NE. Hilbert-Huang transform and its applications. World Scientific; 2014.

Huang, NE., Shen, Z., Long, SR., Wu, MC., Shih, HH., Zheng, Q., Yen, N-C., Tung, CC., Liu, HH. Proceedings of the Royal Society of London A: mathematical, physical and engineering sciences. The Royal Society; 1998. The empirical mode decomposition and the Hilbert spectrum for nonlinear and non-stationary time series analysis.

Hughes SW, Crunelli V. Thalamic mechanisms of EEG alpha rhythms and their pathological implications. The Neuroscientist. 2005; 11(4):357–372. [PubMed: 16061522]

Izhikevich EM. Simple model of spiking neurons. IEEE Transactions on neural networks. 2003; 14(6): 1569–1572. [PubMed: 18244602]

Izhikevich, EM. Dynamical systems in neuroscience. MIT press; 2007.

Jackson MP, Rahman A, Lafon B, Kronberg G, Ling D, Parra LC, Bikson M. Animal models of transcranial direct current stimulation: Methods and mechanisms. Clinical Neurophysiology. 2016; 127(11):3425–3454. [PubMed: 27693941]

Jensen MH, Bak P, Bohr T. Complete devil's staircase, fractal dimension, and universality of mode-locking structure in the circle map. Physical review letters. 1983; 50(21):1637.

Kasten FH, Dowsett J, Herrmann CS. Sustained Aftereffect of α-tACS Lasts Up to 70 min after Stimulation. Frontiers in human neuroscience. 2016; 10

Kasten FH, Herrmann CS. Transcranial alternating current stimulation (tACS) enhances mental rotation performance during and after stimulation. Frontiers in Human Neuroscience. 2017; 11

Klimesch W. EEG alpha and theta oscillations reflect cognitive and memory performance: a review and analysis. Brain research reviews. 1999; 29(2):169–195. [PubMed: 10209231]

Klimesch W, Sauseng P, Hanslmayr S. EEG alpha oscillations: the inhibition–timing hypothesis. Brain research reviews. 2007; 53(1):63–88. [PubMed: 16887192]

Lachaux JP, Rodriguez E, Martinerie J, Varela FJ. Measuring phase synchrony in brain signals. Human brain mapping. 1999; 8(4):194–208. [PubMed: 10619414]

Lafon B, Rahman A, Bikson M, Parra LC. Direct Current Stimulation alters neuronal input/output function. Brain Stimulation. 2016

Longtin A, Middleton JW, Cieniak J, Maler L. Neural dynamics of envelope coding. Mathematical biosciences. 2008; 214(1):87–99. [PubMed: 18514744]

Lopez L, Chan CY, Okada Y, Nicholson C. Multimodal characterization of population responses evoked by applied electric field in vitro: extracellular potential, magnetic evoked field, transmembrane potential, and current-source density analysis. The Journal of Neuroscience. 1991; 11(7):1998–2010. [PubMed: 2066771]

Lowet E, Roberts MJ, Bonizzi P, Karel J, De Weerd P. Quantifying Neural Oscillatory Synchronization: A Comparison between Spectral Coherence and Phase-Locking Value Approaches. PloS one. 2016; 11(1):e0146443. [PubMed: 26745498]

Lundstrom BN, Fairhall AL. Decoding stimulus variance from a distributional neural code of interspike intervals. Journal of Neuroscience. 2006; 26(35):9030–9037. [PubMed: 16943561]

Lustenberger C, Boyle MR, Foulser AA, Mellin JM, Fröhlich F. Functional role of frontal alpha oscillations in creativity. Cortex. 2015; 67:74–82. [PubMed: 25913062]

Markram H, Toledo-Rodriguez M, Wang Y, Gupta A, Silberberg G, Wu C. Interneurons of the neocortical inhibitory system. Nature Reviews Neuroscience. 2004; 5(10):793–807. [PubMed: 15378039]

Marshall L, Binder S. Contribution of transcranial oscillatory stimulation to research on neural networks: an emphasis on hippocampo-neocortical rhythms. Frontiers in human neuroscience. 2013; 7

Mazzoni A, Lindén H, Cuntz H, Lansner A, Panzeri S, Einevoll GT. Computing the local field potential (LFP) from integrate-and-fire network models. PLOS Comput Biol. 2015; 11(12):e1004584. [PubMed: 26657024]

Mazzoni A, Panzeri S, Logothetis NK, Brunel N. Encoding of naturalistic stimuli by local field potential spectra in networks of excitatory and inhibitory neurons. PLoS Comput Biol. 2008; 4(12):e1000239. [PubMed: 19079571]

Middleton JW, Longtin A, Benda J, Maler L. The cellular basis for parallel neural transmission of a high-frequency stimulus and its low-frequency envelope. Proceedings of the National Academy of Sciences. 2006; 103(39):14596–14601.

Mitra, P., Bokil, H. Observed Brain Dynamics. Oxford University Press; Oxford: 2008.

Naka A, Adesnik H. Inhibitory circuits in cortical layer 5. Frontiers in neural circuits. 2016; 10

Neuling T, Rach S, Herrmann CS. Orchestrating neuronal networks: sustained after-effects of transcranial alternating current stimulation depend upon brain states. Frontiers in human neuroscience. 2013; 7

Nunez, PL., Srinivasan, R. Electric fields of the brain: the neurophysics of EEG. Oxford University Press; USA: 2006.

Ozen S, Sirota A, Belluscio MA, Anastassiou CA, Stark E, Koch C, Buzsaki G. Transcranial electric stimulation entrains cortical neuronal populations in rats. J Neurosci. 2010; 30(34):11476–11485. [PubMed: 20739569]

Percival, DB., Walden, AT. Spectral analysis for physical applications. Cambridge University Press; 1993.

Pikovsky, A., Rosenblum, M., Kurths, J. Synchronization: a universal concept in nonlinear sciences. Cambridge university press; 2003.

Radman T, Ramos RL, Brumberg JC, Bikson M. Role of cortical cell type and morphology in subthreshold and suprathreshold uniform electric field stimulation in vitro. Brain stimulation. 2009; 2(4):215–228. e213. [PubMed: 20161507]

Radman T, Su Y, An JH, Parra LC, Bikson M. Spike timing amplifies the effect of electric fields on neurons: implications for endogenous field effects. The Journal of Neuroscience. 2007; 27(11): 3030–3036. [PubMed: 17360926]

Reato D, Bikson M, Parra LC. Lasting modulation of in vitro oscillatory activity with weak direct current stimulation. Journal of neurophysiology. 2015; 113(5):1334–1341. [PubMed: 25505103]

Reato D, Rahman A, Bikson M, Parra LC. Low-intensity electrical stimulation affects network dynamics by modulating population rate and spike timing. Journal of Neuroscience. 2010; 30(45): 15067–15079. [PubMed: 21068312]

Reato D, Rahman A, Bikson M, Parra LC. Low-intensity electrical stimulation affects network dynamics by modulating population rate and spike timing. J Neurosci. 2010; 30(45):15067–15079. [PubMed: 21068312]

Reato D, Rahman A, Bikson M, Parra LC. Effects of weak transcranial alternating current stimulation on brain activity—a review of known mechanisms from animal studies. Frontiers in human neuroscience. 2013; 7

Ruhnau P, Neuling T, Fusca M, Herrmann CS, Demarchi G, Weisz N. Eyes wide shut: Transcranial alternating current stimulation drives alpha rhythm in a state dependent manner. Sci Rep. 2016; 6:27138. [PubMed: 27252047]

Saalmann YB, Pinsk MA, Wang L, Li X, Kastner S. The pulvinar regulates information transmission between cortical areas based on attention demands. Science. 2012; 337(6095):753–756. [PubMed: 22879517]

Santarnecchi E, Polizzotto NR, Godone M, Giovannelli F, Feurra M, Matzen L, Rossi A, Rossi S. Frequency-dependent enhancement of fluid intelligence induced by transcranial oscillatory potentials. Current Biology. 2013; 23(15):1449–1453. [PubMed: 23891115]

Schmidt SL, Iyengar AK, Foulser AA, Boyle MR, Fröhlich F. Endogenous cortical oscillations constrain neuromodulation by weak electric fields. Brain stimulation. 2014; 7(6):878–889. [PubMed: 25129402]

Tergau F, Paulus W. Neuroplasticity induced by transcranial direct current stimulation. Oxford handbook of transcranial stimulation. 2008:201.

Traub RD, Contreras D, Cunningham MO, Murray H, LeBeau FE, Roopun A, Bibbig A, Wilent WB, Higley MJ, Whittington MA. Single-column thalamocortical network model exhibiting gamma oscillations, sleep spindles, and epileptogenic bursts. Journal of neurophysiology. 2005; 93(4): 2194–2232. [PubMed: 15525801]

Turi Z, Ambrus G, Janacsek K, Emmert K, Hahn L, Paulus W, Antal A. Both the cutaneous sensation and phosphene perception are modulated in a frequency-specific manner during transcranial alternating current stimulation. Restorative neurology and neuroscience. 2013; 31(3):275–285. [PubMed: 23478342]

Vossen A, Gross J, Thut G. Alpha power increase after transcranial alternating current stimulation at alpha frequency (α-tACS) reflects plastic changes rather than entrainment. Brain stimulation. 2015; 8(3):499–508. [PubMed: 25648377]

Witkowski M, Garcia-Cossio E, Chander BS, Braun C, Birbaumer N, Robinson SE, Soekadar SR. Mapping entrained brain oscillations during transcranial alternating current stimulation (tACS). Neuroimage. 2016; 140:89–98. [PubMed: 26481671]

Yoshimura Y, Callaway EM. Fine-scale specificity of cortical networks depends on inhibitory cell type and connectivity. Nature neuroscience. 2005; 8(11):1552–1559. [PubMed: 16222228]

Zaehle T, Rach S, Herrmann CS. Transcranial alternating current stimulation enhances individual alpha activity in human EEG. PloS one. 2010; 5(11):e13766. [PubMed: 21072168]

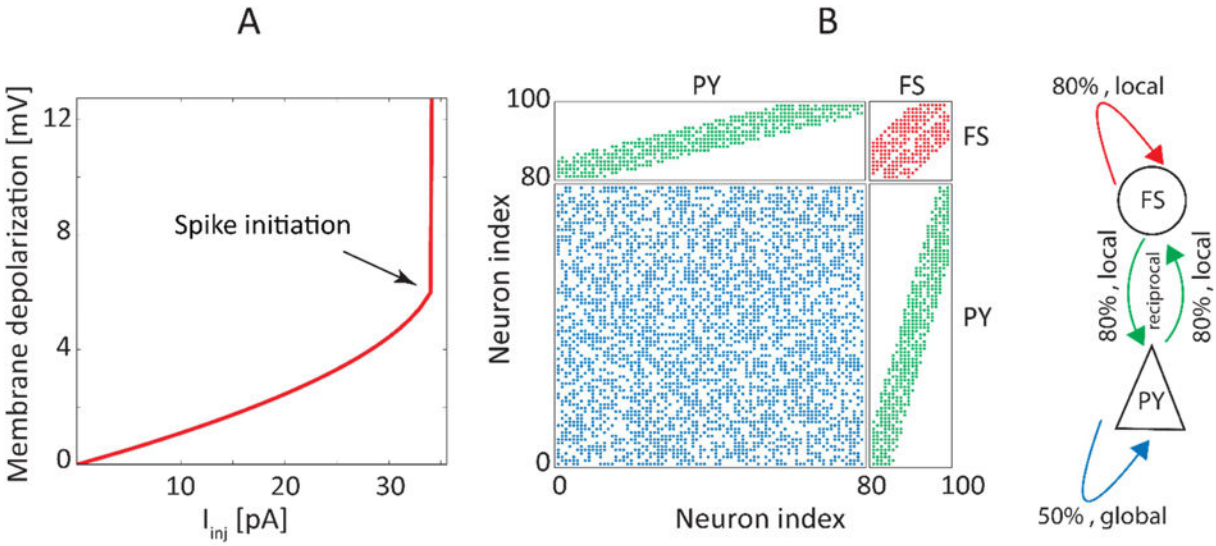

Figure 1.

Pyramidal neuron response to dc current injection and network structure and connection pattern. (**A**) Membrane depolarization of a pyramidal model neuron in response to current injection. Subthreshold current injections (I_{inj}<34 pA) resulted in small membrane depolarization. (**B**)The network was composed of 80 regular spiking excitatory pyramidal cells (PY) and 20 fast spiking inhibitory cells (FS). The PY had a global connectivity with connection probability of 50% (blue dots). The FS were randomly connected to 80% of 10 adjacent FS (red dots). The PY-FS followed a reciprocal local connection (green dots) where every FS was randomly connected to 80% of 32 surrounding PY neurons.

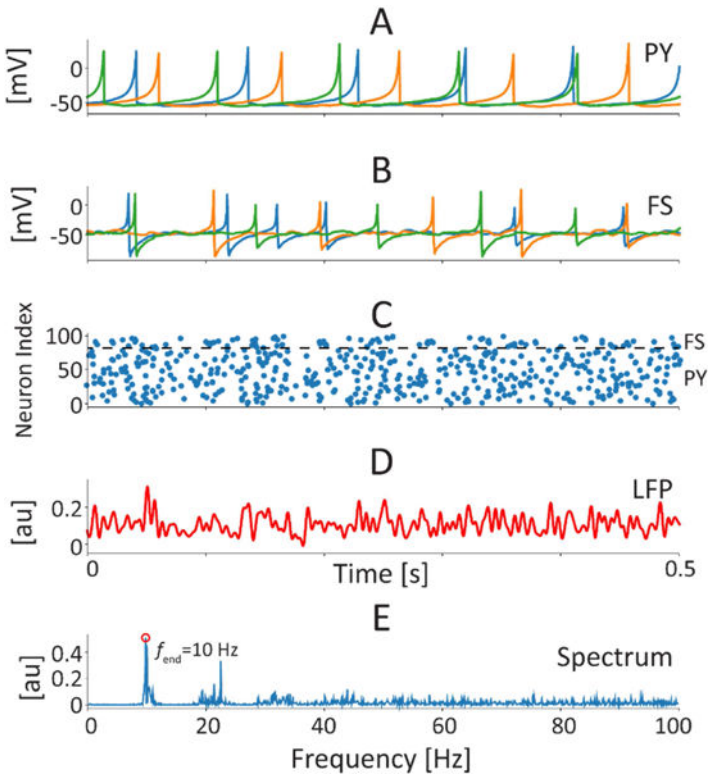

Figure 2.

Single-neuron and network dynamics in absence of stimulation. (**A**, **B**): pyramidal cells (PY) and fast spiking inhibitory cells (FS) membrane voltage traces. Different colors represent different neurons. Each neuron fired about 10 spikes per second. (**C**): Raster plot of spiking activity across all neurons with each dot representing the spike time of the corresponding neuron. (**D**, **E**): The extracted local field potential (LFP) signal and corresponding power spectrum with a peak at f_{end}= 10 Hz.

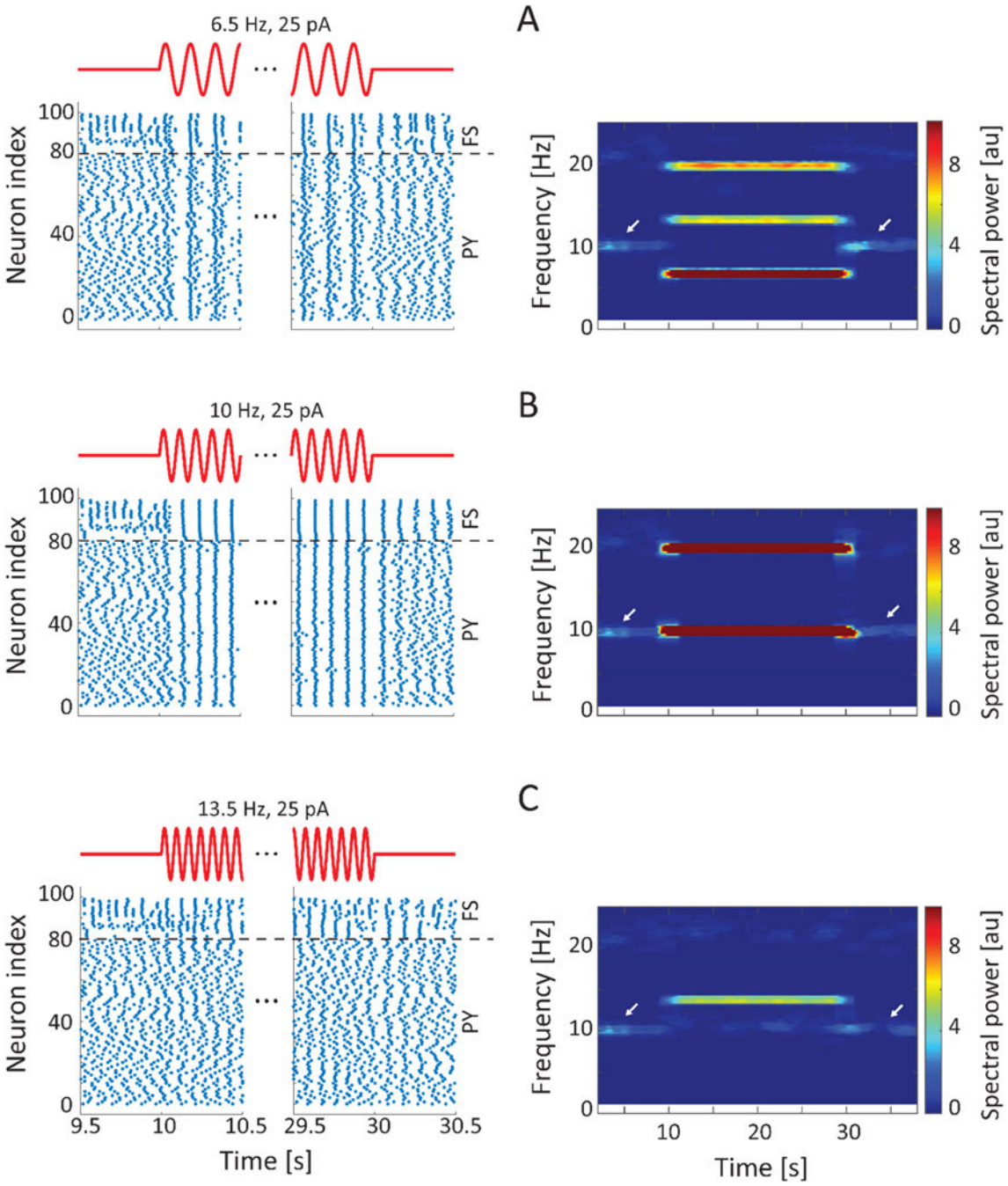

Figure 3.

Transcranial alternating current stimulation (tACS) modulates the ongoing network activity. (A, B, C): The spiking activity of individual neurons (blue dots) in response to 6.5, 10, 13.5 Hz tACS respectively (left column). The white arrows in the time-frequency representations show the ongoing 10 Hz oscillations in the absence of stimulation (right column). The tACS modulated ongoing activity by changing the oscillation frequency (A, C) or amplifying the ongoing oscillations (B) as shown by spectrograms of the corresponding local field potential signals. Stimulation was turned on at $t = 10$ sec and lasted for 20 seconds.

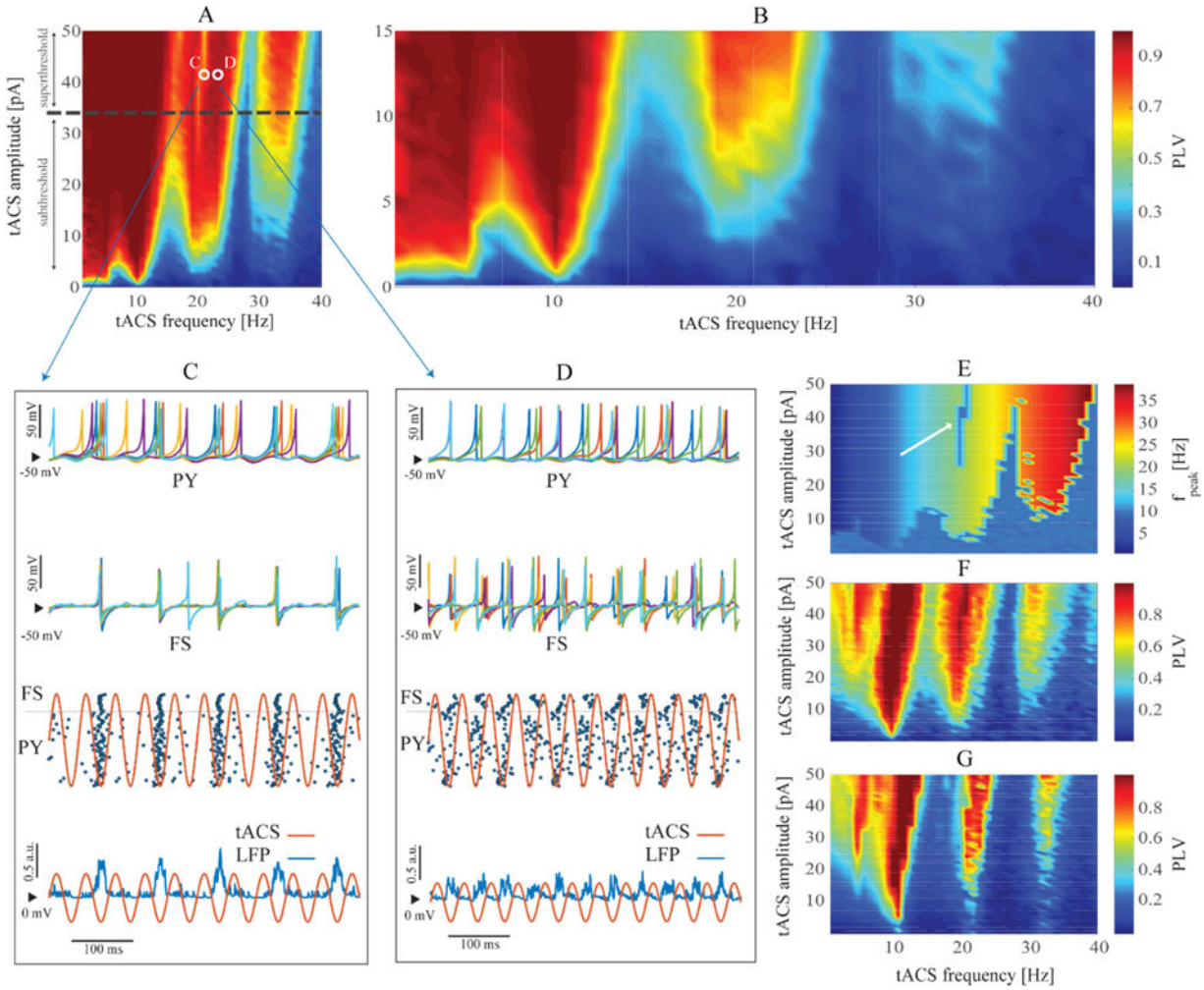

Figure 4.

Entrainment of individual neurons and network oscillations by conventional transcranial alternating current stimulation (tACS). (**A, B**) Entrainment map of the local field potential (LFP) to unmodulated low-frequency tACS. The vertical and horizontal axes display the stimulation parameters. The color corresponded to the phase locking value (PLV) between conventional tACS and LFP for each stimulation frequency-intensity pair. The dashed line at $I = 34$ pA indicated the maximum subthreshold intensity of conventional tACS. (**C**, **D**) Network dynamics over a 0.5-sec period at two selected points on PLV heat map indicated by open white circles in (**A**) corresponding to tACS frequency and amplitude of [21 Hz, 44.1 pA] and [23 Hz, 44.1 pA] respectively. The pyramidal (PY) and fast-spiking (FS) neurons fired in synchrony in (**C**) resulting in a 10 Hz population activity as indicated by raster plot (second bottom) and resulting local field potential (LFP) signal (bottom). The less synchronous firing of individual neurons in (**D**) resulted in a 20 Hz population activity. The amplitude of tACS traces (orange sinusoidal traces in **C**, **D**) was scaled for visualization purpose. (**E**) Network peak frequency map as a function of stimulation parameters. (**F**, **G**) Phase locking value of two randomly selected individual pyramidal neurons to stimulation waveform as a function of stimulation parameters.

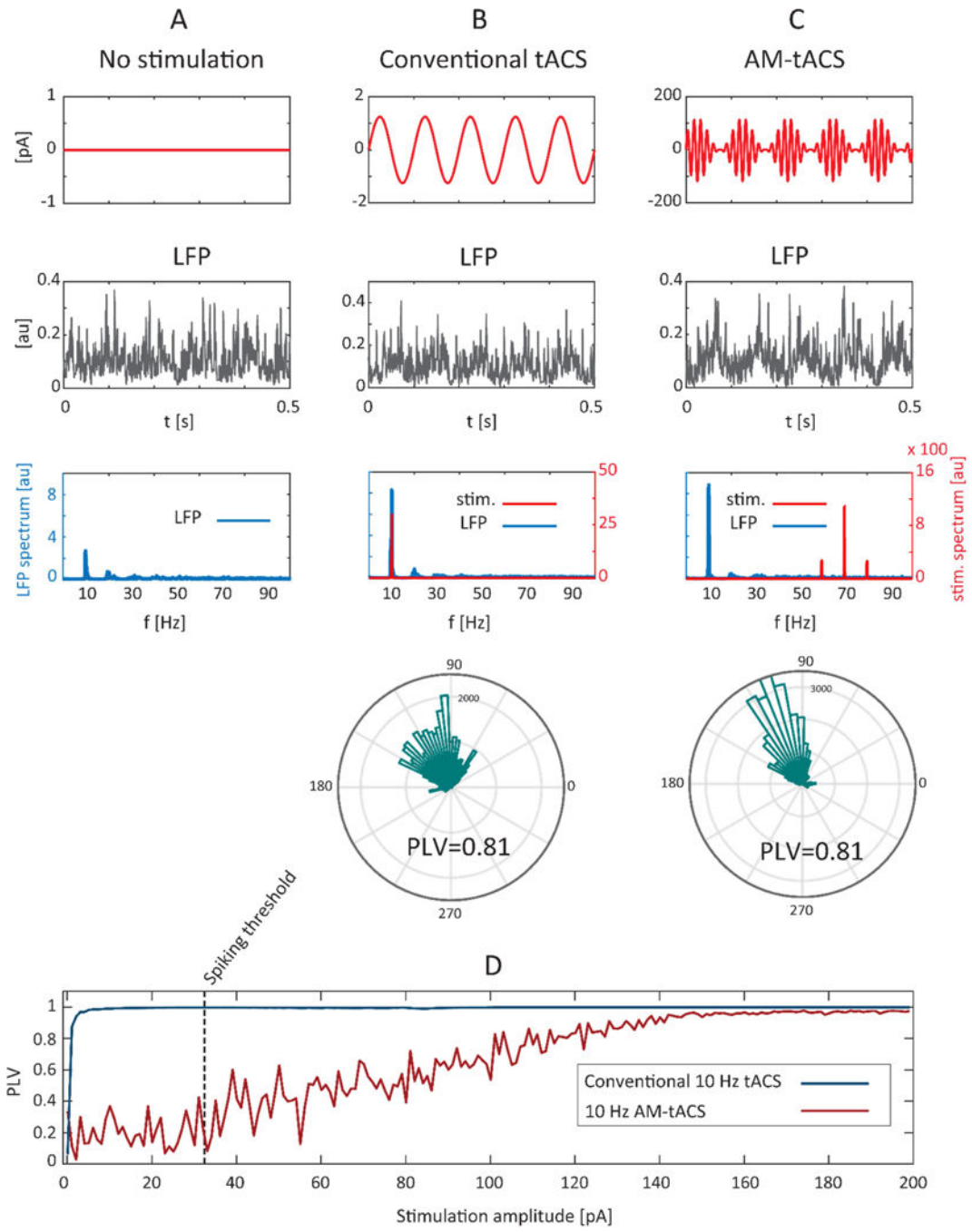

Figure 5.

Comparing the effect of amplitude-modulated transcranial alternating current stimulation (AM-tACS) with unmodulated low-frequency transcranial alternating current stimulation (tACS) on alpha-band cortical oscillations. (**A**): Ongoing cortical activity without stimulation with a prominent spectral peak at 10 Hz. (**B**): Network response to a 10 Hz unmodulated tACS with amplitude of 1.25 pA showing an increased spectral power at 10 Hz. The circular histogram of phase differences between conventional tACS and LFP shows phase synchronization with corresponding phase locking value of PLV=0.81. (**C**): Network

response to AM-tACS with modulating and carrier frequencies of f_m = 10 Hz and f_c = 70 Hz respectively. The AM-tACS with amplitude of 118.5 pA resulted in PLV=0.81. (**D**): The PLV versus stimulation amplitude for conventional tACS and AM-tACS. The dashed line at I = 34 pA indicates the current intensity required to elicit firing of pyramidal neurons.

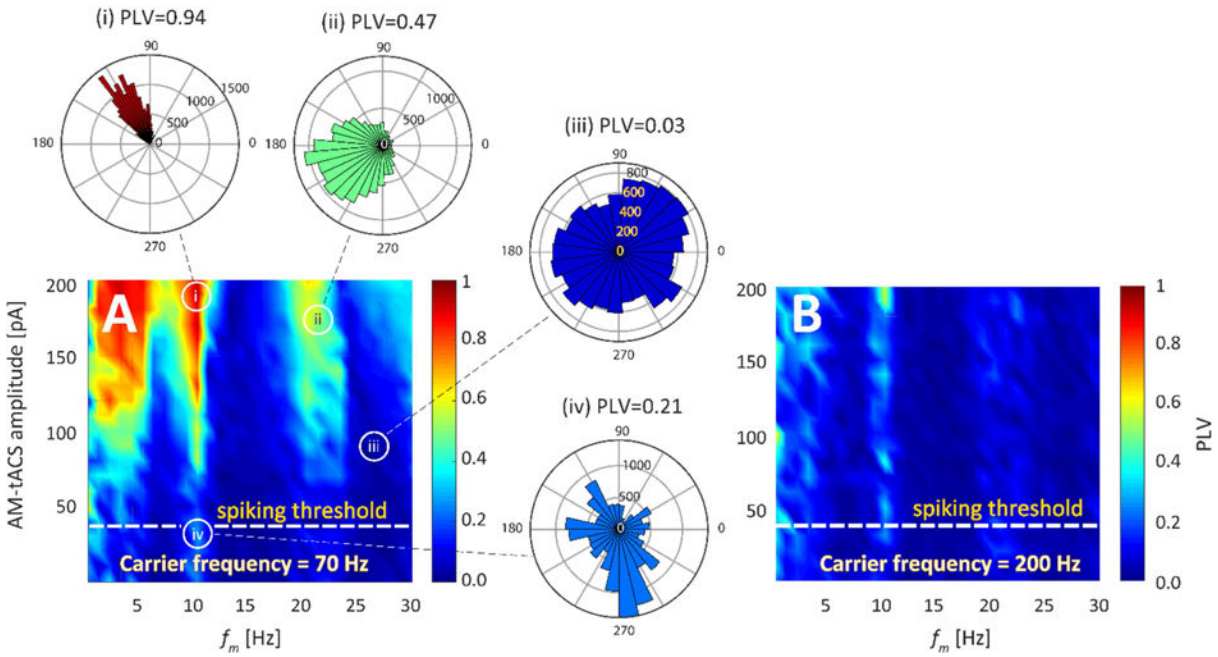

Figure 6.

Entrainment map of the local field potential (LFP) by amplitude modulated (AM) stimulation. The maps show the phase locking value (PLV) between modulation frequency of stimulation and LFP at each stimulation frequency and intensity pair. (**A**): The carrier frequency is f_c = 70 Hz. Highly synchronized triangular region emerged at f_{end} = 10 Hz. High-PLV regions were also evident at subharmonic and harmonic frequencies. Dashed line was the spiking threshold for current intensity at I=34 pA. Circular histogram of phase differences between AM-tACS waveform and LFP was demonstrated for four selected points (i-iv) showing different degrees of phase locking. (**B**): The carrier frequency is f_c Hz. = 200 Hz. Weaker phase locking developed at f_{end} = 10 Hz and its first harmonic, without showing a clear triangular shape.

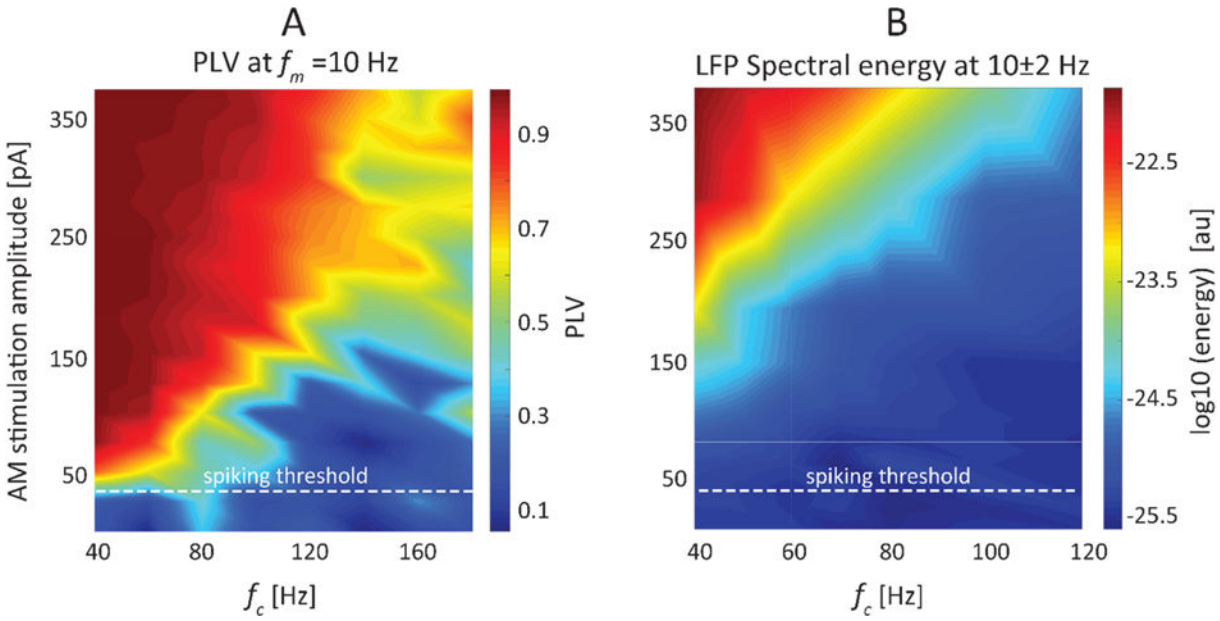

Figure 7.

Effect of the carrier frequency (f_C) on interaction between amplitude-modulated (AM) stimulation and the local field potential (LFP). (**A**) Phase locking value is color coded for different carrier frequencies and AM-tACS amplitudes. Higher carrier frequencies require larger stimulus amplitudes to result in strong phase synchronization. (**B**) spectral energy of LFP within a 10±2 Hz band is color coded as a function of carrier frequency and amplitude of MA-tACS indicating reduced LFP energies delivered by higher carrier frequencies. The modulating frequency was fixed at f_m = 10 Hz. The spiking threshold for stimulus intensity is indicated by dashed line.